ICCFD13
MILAN ITALY 2026

Numerical Investigation of Solid-Solid Phase Change Material for Thermal Management of Lithium-Ion Batteries Under Aggressive Discharging-Charging Cycles

Vanita A. Wagh* and Sandip K. Saha*
Corresponding author: vanitawagh13@gmail.com
* Department of Mechanical Engineering, Indian Institute of Technology Bombay, Mumbai-400076, India.

Abstract

Lithium-ion batteries (LIBs) in electric vehicles require effective thermal management, particularly under high C-rate operations in hot environments. While solid-liquid phase change materials (SL-PCMs) such as n-docosane, when integrated with cooling channels, offer effective thermal regulation, their requirement for complete resolidification between aggressive discharge-charging cycles poses a critical operational constraint. This study investigates neopentyl glycol (NPG), a solid-solid phase change material (SS-PCM), as an alternative to n-docosane for thermal management of a Samsung ICR 18650-26J lithium-ion battery. A three-dimensional numerical model based on the Multi-Scale Multi-Domain (MSMD) approach with the Newman-Tiedemann-Gu-Kim (NTGK) electrochemical model is employed to simulate the thermal behaviour during 3C discharging followed by 1C charging at 40 °C. The effects of NPG thickness (3–4 mm) and ambient temperature (30–40 °C) on cell temperature and phase fraction are systematically evaluated. A direct comparison between NPG (latent heat: 126 kJ/kg) and n-docosane (latent heat: 257 kJ/kg) reveals that while docosane achieves lower peak cell temperatures in a single cycle, NPG eliminates the resolidification requirement entirely by undergoing a reversible solid-solid phase transition. This characteristic makes NPG particularly advantageous for sustained multi-cycle operation in hot climates, where incomplete SL-PCM recovery progressively degrades thermal performance.

Keywords: Solid-Solid PCM, Neopentyl Glycol, Lithium-Ion Battery, Thermal Management, NTGK Model, Discharging- Charging Cycle.

1. Introduction

Electric vehicles (EVs) have emerged as a sustainable alternative to internal combustion engines, driven by their reduced environmental impact and energy efficiency [1]. Lithium-ion batteries (LIBs), the primary energy storage component in EVs, are favoured for their high energy density, long cycle life, and eco-friendly attributes [2]. However, LIBs are highly sensitive to temperature, with an optimal operating range of 15 to 45 °C. During high C-rate charge and discharge operations, substantial heat is generated, which can drive cell temperatures beyond safe limits, leading to accelerated capacity degradation, non-uniform temperature distributions, and in extreme cases, thermal runaway [3], [4]. A cylindrical 18650 cell without cooling can exceed 45 °C at discharge rates of 1C to 5C [12]. Consequently, effective battery thermal management systems (BTMS) are critical for ensuring the safety, performance, and lifespan of LIBs, particularly in hot climates such as India and the Middle East, where ambient temperatures can reach 40 °C or higher [5].

Phase change materials (PCMs) have gained significant attention for battery thermal management due to their ability to absorb large quantities of heat during phase transitions at nearly constant temperature [6], [7]. Solid-liquid PCMs (SL-PCMs), particularly paraffins such as n-docosane, offer high latent heat of fusion (approximately 257 kJ/kg) and phase transition temperatures well-suited for LIB applications (approximately 42–45 °C) [8]. However, standalone SL-PCMs suffer from inherently low thermal

conductivity (typically 0.2–0.3 W/m·K), liquid leakage after melting, and the need for containment structures [9]. To overcome these limitations, hybrid BTMS designs combining PCMs with active cooling strategies have been extensively investigated. Wagh and Saha [8] optimised extended fin configurations integrated with PCM to enhance heat transfer and reduce peak battery temperatures by up to 40.63 °C during 3C discharge at 40 °C ambient. Their subsequent work [10] identified the optimal heat transfer coefficient required for complete PCM solidification during the charging phase following high-rate discharge, demonstrating that n-docosane can achieve full solidification within 750 s at a convective heat transfer coefficient of 500 W/m²·K.

A critical operational challenge in PCM-based BTMS is the requirement for complete resolidification of the SL-PCM before the next discharging cycle begins. Under aggressive cycling conditions (3C discharge followed by 1C charge at 40 °C ambient), the SL-PCM must transition from liquid back to solid, and any residual liquid fraction carries over to the subsequent cycle, progressively degrading thermal management effectiveness [11]. Wagh and Saha [11] demonstrated that increasing the heat transfer coefficient from 50 to 200 W/m²·K reduces the PCM recovery time by 42.7% in a novel battery-PCM-channel configuration with immersion cooling. Their thermal resistance analysis revealed that the thermal conductivity of the PCM itself remains the limiting factor for heat dissipation [12]. Despite these advances, the resolidification requirement remains a fundamental bottleneck for SL-PCMs under continuous aggressive cycling. The liquid phase introduces additional complications, including density-driven natural convection, orientation dependence, and leakage risk that complicate system design and reliability [13], [14].

Solid-solid phase change materials (SS-PCMs) present an attractive alternative that eliminates the resolidification constraint entirely. SS-PCMs undergo reversible crystalline phase transitions in the solid state, absorbing and releasing latent heat without forming a liquid phase [15]. Among SS-PCMs, polyalcohols such as neopentyl glycol (NPG), pentaerythritol (PE), and trimethylolaminomethane (TAM) are commonly preferred due to their relatively high transition enthalpies [16]. NPG is a particularly promising candidate, exhibiting a solid-solid phase transition from an ordered monoclinic crystal structure to an orientationally disordered face-centred cubic (FCC) structure at approximately 42–48 °C, with a latent heat of approximately 126 kJ/kg [17]. The key advantages of SS-PCMs over SL-PCMs include no liquid leakage, minimal volume change during transition, no orientation dependence, elimination of encapsulation requirements, and excellent thermal cycling stability [15], [18]. The principal trade-off is their lower latent heat capacity compared to SL-PCMs.

Recent studies have explored NPG-based SS-PCMs primarily for electronics cooling applications. Wang et al. [17] demonstrated that NPG saturated into compressed, expanded natural graphite matrices can achieve thermal conductivity enhancements of 11-88 times compared to pure NPG. Praveen and Suresh [19] experimentally investigated an NPG/CuO composite SS-PCM in a heat sink for electronic cooling, achieving a 4.08-fold improvement in thermal conductivity. Midhun et al. [18] conducted a numerical investigation and optimisation of SS-PCM-based plate--fin heat sinks for electronic packages using the effective heat capacity method, while Midhun and Saha [20] investigated SS-PCM composite heat sinks with tandem coupled heat pipes to manage safe operational time in thermally hostile environments. Serrano et al. [21] explored NPG-docosane composites as shape-stabilised PCMs, demonstrating combined latent heats of up to 210.74 J/g. However, the application of SS-PCMs, particularly NPG, for lithium-ion battery thermal management has not been investigated to date.

The present study addresses this gap by numerically investigating NPG as an SS-PCM for thermal management of a Samsung ICR 18650-26J lithium-ion battery in a copper shell-PCM configuration established in prior work [8], [11]. A three-dimensional numerical model based on the MSMD-NTGK framework is employed to simulate the thermal behaviour under 3C discharging followed by 1C charging at 40 °C ambient temperature. The objectives of this study are: (i) to evaluate the effect of NPG thickness on cell temperature and phase fraction; (ii) to assess the influence of ambient temperature on NPG thermal performance; and (iii) to directly compare the thermal performance of NPG (SS-PCM) with n-docosane (SL-PCM) at different thicknesses, thereby quantifying the trade-off between latent heat capacity and the elimination of the re-solidification constraint.

2. Methodology

The study utilizes a SAMSUNG ICR 18650-26J Lithium-ion battery with a nominal capacity of 2600 mAh. Fig. 1 illustrates the battery structure, which includes an 18 mm diameter core encased by a 0.5 mm thick inner copper shell. This core-shell assembly is then surrounded by a 3 mm layer of PCM and further protected by a 0.5 mm outer copper shell. Additionally, both the top and bottom of the battery are fitted with 1 mm thick caps. Table 1 details the battery's operating parameters, while Table 2 lists material properties, such as thermal conductivity, that affect heat dissipation in lithium-ion batteries.

Two phase change materials are investigated in this study: n-docosane, a solid-liquid PCM (SL-PCM), and neopentyl glycol (NPG), a solid-solid PCM (SS-PCM). N-docosane is a widely used paraffin wax with a melting temperature of approximately 42–44 °C and a high latent heat of fusion of 257 kJ/kg [8], [9]. During phase transition, docosane undergoes a complete solid-to-liquid transformation, requiring the solution of the continuity, momentum, and energy equations using the enthalpy-porosity method to capture mushy-zone dynamics and buoyancy-driven natural convection in the liquid phase. NPG is a polyhydric alcohol that undergoes a reversible solid-solid phase transition from an ordered monoclinic crystal structure to an orientationally disordered face-centred cubic (FCC) structure at approximately 42.4 °C, with a latent heat of 126 kJ/kg [16], [17]. Since no liquid phase forms during the NPG transition, only the energy equation is solved, employing the effective heat capacity method to account for latent heat absorption and release over a narrow transition temperature range [18], [20].

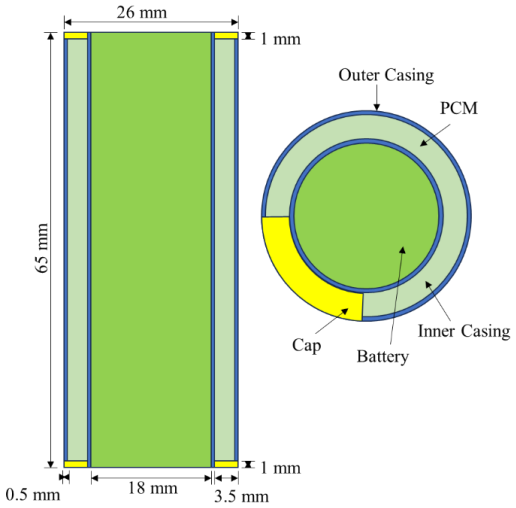

Figure 1: Battery encased with copper shells and PCM.

TABLE 1 Specification and material properties of Samsung 18650 LIB

Parameter	Value
Nominal voltage (V)	3.7
Minimum stop voltage (V)	2.8
Maximum stop voltage (V)	4.2
Cell weight (gm)	43.87
Nominal capacity (mAh)	2600
Electrolyte type	Carbonate based
Cathode type	Lithium Cobalt Oxide (LiCoO2)
Anode type	Graphite
Specific heat capacity of the positive tab (J/kg·K)	871

Density of the positive tab (kg/m³)	2719
Thermal conductivity of the positive tab (W/m·K)	202
Specific heat capacity of the negative tab (J/kg·K)	381
Density of the negative tab (kg/m³)	8978
Thermal conductivity of the negative tab (W/m·K)	387.6
Thermal conductivity of the cell (W/m·K): radial, tangential, axial	3.4, 24, 24
Specific heat capacity of the cell (J/kg·K)	871

TABLE 2 Thermophysical properties of n-Docosane [23], NPG [21], and copper [24]

Property	n-Docosane	NPG	Copper
Density (kg/m³)	778	1060	8978
Reference temperature (°C)	42.1	-	-
Volumetric thermal expansion coefficient (K^{-1})	1×10^{-5}	-	-
Thermal conductivity (W/m·K)	0.21	0.25	387.6
Melting point (°C)	44.7	42.4	-
Latent heat of fusion (J/kg)	257000	126000	-
Specific heat capacity (J/kg·K)	2650	1800	381
Dynamic viscosity (kg/m·s)	0.0046	-	-

3 Numerical Model

The numerical model is developed using the MSMD framework coupled with the NTGK model, selected for its capability to reliably represent the thermal and electrical behavior of lithium-ion batteries under different operating conditions. A three-dimensional, cell-level analysis is performed by solving the governing differential equations for coupled thermal and electrical transport within the battery. The model simplifies internal electrochemical complexity by neglecting enthalpy of mixing and phase-change effects inside the cell [25]. The governing equations for current flux at both the positive and negative electrodes are incorporated, establishing a comprehensive framework to describe battery operating characteristics [24,25].

3.1 Conservation of thermal and electrical energy for the battery:

$$\frac{\partial(\rho_B c_B T_B)}{\partial t} = \nabla\cdot\left(K_B \nabla T_B\right) + \sigma_+|\nabla\phi_+|^2 + \sigma_-|\nabla\phi_-|^2 + \dot{q}_{ECh} + \dot{q}_{short} \tag{1}$$

$$\nabla\cdot(\sigma_+\nabla\phi_+) = -(j_{ECh} - j_{short}) \tag{2}$$

$$\nabla\cdot(\sigma_-\nabla\phi_-) = (j_{ECh} - j_{short}) \tag{3}$$

In the above equation, j_{short} and $\dot{q}_{short}$ represent the current transfer rate and heat generation during an internal short circuit; both are zero if no short circuit occurs. j_{ECh} and $\dot{q}_{ECh}$ denote the volumetric current transfer rate and heat generation due to electrochemical reactions. The value of j_{ECh} is calculated using the following equation.

$$j_{ECh} = \frac{Q_{nom}}{Q_{ref} Vol_B} Y[U - V] \tag{4}$$

$$DOD = \frac{Vol_B}{3600 Q_{nom}} \int_0^t j dt \tag{5}$$

In the above equation, V is the cell voltage, Q_{nom} the nominal capacity, and Q_{ref} the experimental reference capacity. The experiments determine the parameters *Y* and *U*, which are coefficients of the depth-of-discharge function [7].

$$\dot{q}_{ECh} = j_{ECh} \left[(U - V) - T \frac{dU}{dt} \right] \tag{6}$$

$$U = a_0 + a_1 DOD^1 + a_2 DOD^2 + a_3 DOD^3 + a_4 DOD^4 \tag{7}$$

$$Y = b_0 + b_1 DOD^1 + b_2 DOD^2 + b_3 DOD^3 + b_4 DOD^4 \tag{8}$$

3.2 Equations for Solid-Liquid PCM:

In this study, the enthalpy method is applied to model PCM melting and solidification. For each computational cell, the total enthalpy (E) is the sum of sensible heat (e) and latent heat (ΔE), i.e.,

$$E = e + \Delta E \tag{9}$$

The liquid fraction of PCM is expressed as,

$$f_l = \frac{\Delta E}{L} \tag{10}$$

The PCM model employs a transient, three-dimensional approach based on the fundamental equations governing both fluid dynamics and heat transfer phenomena. The fluid flow of PCM is assumed to be laminar and Newtonian. The liquid PCM is considered as an incompressible fluid. The shrinkage and expansion effects during phase change are neglected. In the analysis, property values are assumed to remain constant across the temperature range considered in this study. The governing equations delineating the PCM domain, incorporating convective phenomena in the liquid phase, are presented below:

(a) Conservation of mass:

$$\frac{\partial \rho_p}{\partial t} + \nabla . \left(\rho_p \vec{V} \right) = 0 \tag{11}$$

(b) Conservation of momentum:

$$\left(\frac{\partial}{\partial t} + \nabla . \vec{V} \right) \left(\rho_p \vec{V} \right) = -\nabla P + \nabla . \left(\mu \nabla \vec{V} \right) + S_u + S_b \tag{12}$$

where the velocity vector $\vec{V} = u\hat{\imath} + v\hat{\jmath} + w\hat{k}$. The source term S_u is used to model fluid flow during phase change. The configuration includes phases in both solid and liquid form. Another source term S_b signifies the natural convection driven by buoyancy forces.

$$S_u = -A\vec{V} \tag{13}$$

$$S_b = \frac{\rho_p g \beta \left(e - e_{ref} \right)}{c_p} \tag{14}$$

where β is a thermal expansion coefficient and e_{ref} is a reference value of the sensible heat, A denotes the mesh constant, determined by the porosity function.[26]:

$$A = -C \frac{(1 - f_l)^2}{{f_l}^3 + \varepsilon} \qquad 0 < f_l < 1 \tag{15}$$

where C is the porosity constant and is equal to 1.6×10^6 within the semi-liquid region, and ε is a constant taken as 0.001 to avoid division by zero [27].

(c) Conservation of energy equation:

$$\frac{\partial\left(\rho_p c_p T\right)}{\partial \mathrm{t}} + \nabla.\left(\rho_p \vec{V} c_p T\right) = \nabla.\left(K_p \nabla T\right) + S_h \tag{16}$$

where α is the thermal diffusivity and S_h is a phase-related source term and is given by $-\frac{\partial(\rho \Delta E)}{\partial t}$.

3.2.1 Equations for Solid-Solid PCM:

(a) The melt fraction (f_s) of solid-solid PCM is expressed as,

$$f_s = \frac{\Delta E}{L_s} \tag{17}$$

Where, L_s is the latent heat of solid-solid PCM.

(b) Conservation of energy equation for PCM:

$$\frac{\partial\left(\rho_p c_p T\right)}{\partial \mathrm{t}} = \nabla.\left(K_p \nabla T\right) + S_h \tag{18}$$

3.2.2 Initial and boundary conditions:

The initial temperature of both the battery and the PCM is assumed to match the surrounding environment. At the outset, the PCM is in a solid phase, with the velocity field set to zero. The initial condition is given as,

$$\text{At } t = 0;\ T(x,y,z) = T_a = 30\ ℃ \text{ and } \vec{V} = 0 \tag{19}$$

Here, the contact resistance between the cell-copper and PCM-copper surfaces is neglected. The following boundary conditions are used to solve the governing equations.

(a) Copper fin tip:

An adiabatic boundary condition is taken for fin tips, as fin tips are in contact with each other in a battery pack.

$$r = \frac{d_B}{2} + t_{h,cu,i} + t_p + t_{h,cu,o};\ -k_{cu}\frac{\partial T_f}{\partial r} = 0 \tag{20}$$

(b) Copper surface outer to ambient:

Based on Newton's law of cooling, the boundary conditions on the external housing surface to the ambient air are articulated as follows:

$$k_{cu}\frac{\partial T_{cu,o}}{\partial r} = h\left(T_{cu,o} - T_a\right) \tag{21}$$

The interface conditions are set at the interface of different sub-domains, which are written as,

(c) Battery Cell-Copper surface (inner):

$$-k_B\frac{\partial T_B}{\partial r} = -k_{cu}\frac{\partial T_{cu,i}}{\partial r};\ T_B = T_{cu,i} \tag{22}$$

(d) PCM-Copper surface (inner):

$$r = \frac{d_B}{2} + t_{h,cu,i};\ -k_{cu}\frac{\partial T_{cu,i}}{\partial r} = -k_p\frac{\partial T_p}{\partial r};\ T_{cu,i} = T_p \tag{23}$$

(e) PCM-Copper surface (outer):

$$r = \frac{d_B}{2} + t_{h,cu,i} + t_p;\ -k_p \frac{\partial T_p}{\partial r} = -k_{cu} \frac{\partial T_{cu,o}}{\partial r};\ T_p = T_{cu,o} \tag{24}$$

The numerical simulations are performed using the finite volume–based commercial solver ANSYS Fluent 2021 R2 to solve the governing equations. Pressure–velocity coupling is handled using the PISO algorithm, while the PRESTO! scheme is employed for pressure discretization. The momentum and energy equations are discretized using a second-order upwind scheme, and transient effects are captured through a first-order implicit formulation. Convergence criteria are set to 10^{-6} for the energy equation and 10^{-3} for all other variables.

4 Results and Discussion

The numerical results are presented in three parts: the effect of SS-PCM (NPG) thickness, the influence of ambient temperature, and a direct comparison between NPG and n-docosane. All simulations consider a 3C discharging cycle at a convective heat transfer coefficient of h = 20 W/m²·K (representing natural convection), followed by a 1C charging cycle at h = 100 W/m²·K (representing forced convection), consistent with the operating conditions established in [8], [11].

4.1 Effect of SS-PCM (NPG) Thickness

Figure 2 presents the cell and PCM temperature profiles along with the phase fraction evolution for varying NPG thicknesses during a 3C discharging cycle at 40 °C ambient temperature, followed by 1C charging. During the initial phase of 3C discharging, the cell temperature rises rapidly until the NPG reaches its solid-solid transition temperature of approximately 42.4 °C, at which point the rate of temperature rise decreases as latent heat absorption commences. Unlike SL-PCMs, which exhibit a clear temperature plateau during melting, the NPG transition occurs over a narrow temperature range in the solid state. The phase-fraction profiles indicate that thicker NPG layers delay the completion of the solid-solid transition, thereby providing extended thermal buffering.

As the NPG thickness increases from 3 mm to 4 mm, the peak cell temperature during 3C discharging is reduced due to the greater thermal energy storage capacity of the thicker PCM layer. However, the benefit of increasing thickness beyond 4 mm diminishes, consistent with the findings of Wagh and Saha [8] for docosane, where 3 mm was identified as optimal at 30 °C ambient. At 40 °C ambient, the 4 mm thickness represents a practical compromise between thermal performance and system compactness. During the subsequent 1C charging phase, the NPG undergoes a reverse solid-solid transition, returning to its ordered crystalline state. Crucially, this recovery process is entirely governed by conduction, without the complexities of liquid-solid resolidification, mushy zone dynamics, or natural convection effects that characterise SL-PCM recovery [11], [12].

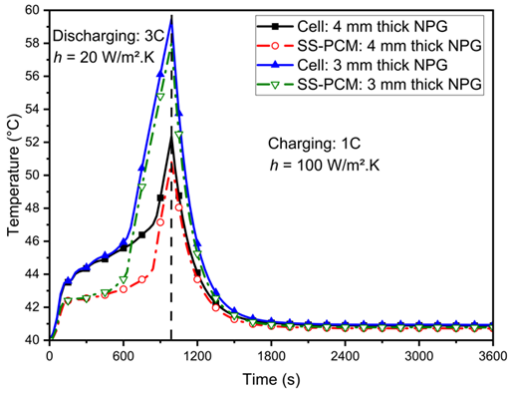

(a)

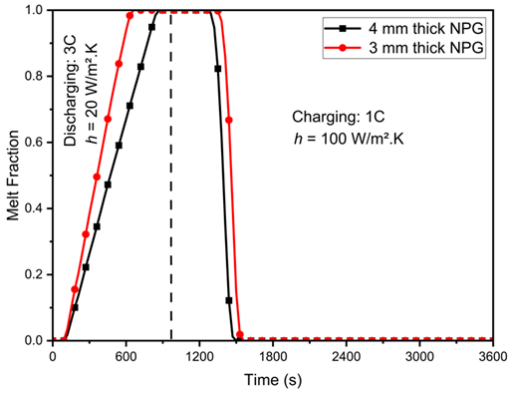

(b)

Figure 2: Effect of SS-PCM (NPG) thickness during a 3C discharging cycle at 40 °C ambient temperature and h = 20 W/m²·K followed by 1C charging with and h = 100 W/m²·K, (a) cell and PCM temperature profiles, (b) liquid fraction profiles.

4.2 Effect of Ambient Temperature

Figure 3 illustrates the effect of ambient temperature (30, 35, and 40 °C) on the thermal performance of 4 mm NPG during a 3C discharging followed by 1C charging cycle. The ambient temperature significantly influences the thermal behaviour through two mechanisms: it determines the initial temperature of the battery and PCM, and it governs the temperature differential available for heat rejection during charging.

At an ambient temperature of 30 °C, the temperature difference between ambient and the NPG transition temperature (approximately 42.4 °C) is approximately 12 °C, providing a substantial driving force for heat rejection and effective PCM recovery during charging. At 35 °C, this differential reduces to approximately 7 °C, and at 40 °C it narrows to only approximately 2 °C. This diminished temperature difference at higher ambient temperatures significantly slows the reverse phase transition rate and limits the extent of phase fraction recovery. This finding is consistent with the observations of Wagh and Saha [10], who reported that at 35 °C ambient, certain SL-PCMs, such as n-heneicosane, remain in the liquid state, whereas n-docosane shows better thermal regulation. For NPG, the absence of a liquid phase means that even at 40 °C ambient, the material remains structurally stable and functional, although its thermal storage utilisation is reduced. The higher density of NPG (1060 kg/m³ compared to 778 kg/m³ for docosane) provides greater volumetric sensible heat storage capacity, partially compensating for the lower latent heat.

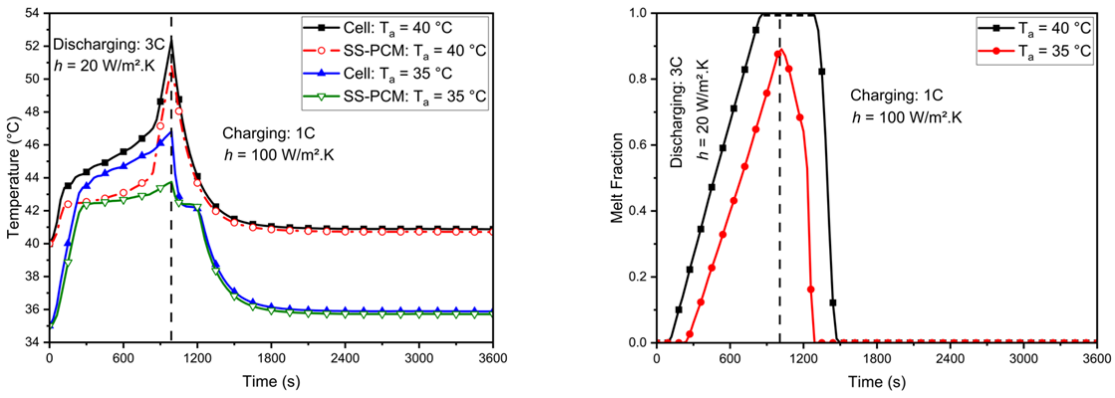

(a) (b)

Figure 3: Effect of ambient temperature during a 3C discharging cycle and h = 20 W/m²·K followed by 1C charging with and h = 100 W/m²·K with 4 mm of NPG, (a) cell and PCM temperature profiles, (b) liquid fraction profiles.

4.3 Comparison of SS-PCM (NPG) and SL-PCM (n-Docosane)

Figure 4 presents the most significant result of this study: a direct comparison between NPG (SS-PCM) and n-docosane (SL-PCM) at different thicknesses during a 3C discharging cycle at 40 °C ambient, followed by 1C charging. The temperature profiles clearly demonstrate the fundamental trade-off between the two materials. Docosane, with its substantially higher latent heat of fusion (257 kJ/kg compared to 126 kJ/kg for NPG), achieves lower peak cell temperatures during the discharging phase due to greater thermal energy absorption capacity during its solid-to-liquid phase transition.

However, the phase fraction profiles reveal a critical distinction. For docosane, the liquid fraction increases during discharging as the material melts. During the subsequent 1C charging phase, the liquid docosane must undergo complete resolidification, a process governed by conduction through the mushy zone, natural convection in the liquid phase, and the temperature differential between the PCM and the

ambient. As demonstrated in [11] and [12], this resolidification is the rate-limiting step in the thermal management cycle, with the thermal resistance of the PCM being the primary bottleneck. At h = 100 W/m²·K during 1C charging, the solidification time for docosane remains considerable, and at 40 °C ambient, the narrow temperature differential further impedes recovery.

For NPG, the phase fraction evolution follows a fundamentally different mechanism. The solid-solid transition from the ordered monoclinic phase to the disordered FCC phase occurs without any liquid formation. The reverse transition during charging is driven purely by conduction, without the complexities of liquid-solid interface dynamics, mushy zone evolution, or buoyancy-driven convection. This difference has profound implications for multi-cycle operation: while docosane requires sufficient time and thermal driving force for complete resolidification before the next discharge cycle, NPG is inherently ready for repeated cycling regardless of the extent of its phase transition. Under aggressive, continuous cycling scenarios in which the time between discharge events is insufficient for complete docosane resolidification, the residual liquid fraction would accumulate progressively, leading to a gradual increase in peak cell temperature across successive cycles [11]. NPG eliminates this failure mode entirely.

It is also noteworthy that NPG has a slightly higher thermal conductivity (0.25 W/m·K) than docosane (0.21 W/m·K) and a significantly higher density (1060 kg/m³ versus 778 kg/m³), translating into greater volumetric thermal energy storage through sensible heating. However, as shown by the thermal resistance analysis in [11], the PCM's thermal conductivity remains the dominant resistance in the heat transfer path, regardless of whether an SS-PCM or an SL-PCM is used. Therefore, thermal-conductivity enhancement strategies, such as the incorporation of expanded graphite [17] or CuO nanoparticles [19], would significantly benefit NPG-based BTMS configurations.

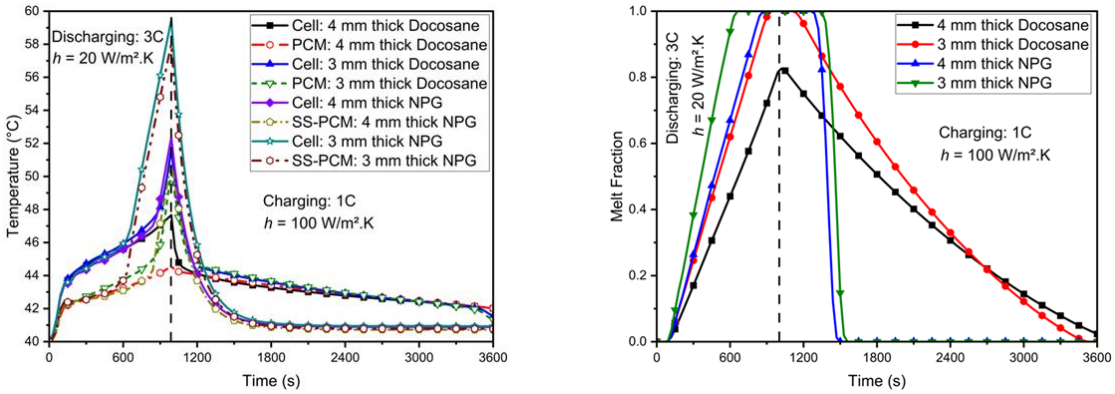

(a) (b)

Figure 4: Comparision of SS-PCM (NPG) and Solid-liquid-PCM (docosane) of different thickness during a 3C discharging cycle at 40 °C ambient temperature and h = 20 W/m²·K followed by 1C charging with and h = 100 W/m²·K, (a) cell and PCM temperature profiles, (b) liquid fraction profiles.

5 Conclusions

This study presents the first numerical investigation of a solid-solid phase change material (neopentyl glycol, NPG) for thermal management of lithium-ion batteries, addressing the critical re-solidification constraint of conventional solid-liquid PCMs. The validated MSMD-NTGK numerical framework is employed to evaluate the thermal performance of NPG in a Samsung ICR 18650-26J battery-copper shell-PCM configuration under 3C discharging followed by 1C charging at 40 °C ambient temperature.

Increasing the NPG thickness from 3 mm to 4 mm reduces the peak cell temperature during 3C discharging, with 4 mm identified as a practical optimum balancing thermal performance and system compactness. The ambient temperature significantly influences NPG performance, with higher ambient temperatures reducing the driving force for heat rejection and slowing phase fraction recovery during

the charging phase. At 40 °C ambient, the narrow temperature differential between the ambient and the NPG transition temperature (approximately 42.4 °C) presents the most challenging operating condition.

The direct comparison of NPG with n-docosane reveals a fundamental trade-off: docosane achieves lower peak cell temperatures in a single discharge cycle due to its higher latent heat (257 kJ/kg vs. 126 kJ/kg). However, NPG eliminates the resolidification requirement entirely, as its reversible solid-solid phase transition does not involve liquid formation, mushy zone dynamics, or natural convection effects. For electric vehicles operating in hot climates with frequent high-rate discharging-charging cycles, where insufficient time exists for complete SL-PCM resolidification, NPG offers a more robust and reliable thermal management solution at the cost of moderately higher peak temperatures.

Future work should focus on enhancing the thermal conductivity of NPG through the incorporation of expanded graphite or CuO nanoparticles, multi-cycle transient analysis comparing NPG and docosane over successive aggressive cycles, integration of NPG with the battery-PCM-channel design for immersion cooling, experimental validation with NPG in the battery-copper shell configuration, and investigation of hybrid SS-PCM/SL-PCM composite configurations.

References

[1] X. Zhang, Z. Li, L. Luo, Y. Fan, and Z. Du, "A review on thermal management of lithium ion batteries for electric vehicles," Energy, vol. 238, p. 121652, 2022.

[2] G. Xia, L. Cao, and G. Bi, "A review on battery thermal management in electric vehicle application," J. Power Sources, vol. 367, pp. 90–105, 2017.

[3] M. M. Khan, M. Alkhedher, M. Ramadan, and M. Ghazal, "Hybrid PCM-based thermal management for lithium-ion batteries: Trends and challenges," J. Energy Storage, vol. 73, p. 108775, 2023.

[4] L. H. J. Raijmakers, D. L. Danilov, R.-A. Eichel, and P. H. L. Notten, "A review on various temperature-indication methods for Li-ion batteries," Appl. Energy, vol. 240, pp. 918–945, 2019.

[5] W. Wu, S. Wang, W. Wu, K. Chen, S. Hong, and Y. Lai, "A critical review of battery thermal performance and liquid based battery thermal management," Energy Convers. Manag., vol. 182, pp. 262–281, 2019.

[6] R. Sabbah, R. Kizilel, J. R. Selman, and S. Al-Hallaj, "Active (air-cooled) vs. passive (phase change material) thermal management of high power lithium-ion packs," J. Power Sources, vol. 182, no. 2, pp. 630–638, 2008.

[7] K. Jiang, G. Liao, E. Jiaqiang, F. Zhang, J. Chen, and E. Leng, "Thermal management technology of power lithium-ion batteries based on the phase transition of materials: a review," J. Energy Storage, vol. 32, p. 101816, 2020.

[8] V. A. Wagh and S. K. Saha, "Optimising extended fin design and heat transfer coefficient for improved heat transfer and PCM recovery time in thermal management of batteries," Appl. Therm. Eng., vol. 255, p. 123964, 2024.

[9] A. Serrano, J.-L. Dauvergne, S. Doppiu, and E. Palomo Del Barrio, "Neopentyl glycol as active supporting media in shape-stabilized PCMs," Materials, vol. 12, no. 19, p. 3169, 2019.

[10] V. A. Wagh and S. K. Saha, "Effect of heat transfer coefficients in forced convective cooling of batteries on the sustained performance of PCMs," J. Fluid Flow Heat Mass Transf., vol. 12, p. 002, 2025.

[11] V. A. Wagh and S. K. Saha, "Novel thermal management design for batteries using PCM and immersion cooling for controlled recovery time under high ambient temperatures," J. Energy Storage, vol. 141, p. 119466, 2026.

[12] V. A. Wagh and S. K. Saha, "On estimating critical channel number of hybrid battery thermal management system combining phase change material and forced convective immersion cooling," Int. Commun. Heat Mass Transf., vol. 171, p. 110114, 2026.

[13] S. K. Saha and P. Dutta, "Effect of melt convection on the optimum thermal design of heat sinks with phase change material," J. Enhanc. Heat Transfer, vol. 18, pp. 249–259, 2011.

[14] S. K. Saha and P. Dutta, "Role of melt convection on optimisation of PCM-based heat sink under cyclic heat load," Heat Transfer Eng., vol. 34, pp. 950–958, 2013.

[15] A. Fallahi, G. Guldentops, M. Tao, S. Granados-Focil, and S. Van Dessel, "Review on solid-solid phase change materials for thermal energy storage: Molecular structure and thermal properties," Appl. Therm. Eng., vol. 127, pp. 1427–1441, 2017.

[16] D. K. Benson, R. W. Burrows, and J. D. Webb, "Solid state phase transitions in pentaerythritol and related polyhydric alcohols," Sol. Energy Mater., vol. 13, pp. 133–152, 1986.

[17] X. Wang, Q. Guo, Y. Zhong, X. Wei, and L. Liu, "Heat transfer enhancement of neopentyl glycol using compressed expanded natural graphite for thermal energy storage," Renew. Energy, vol. 51, pp. 241–246, 2013.

[18] V. C. Midhun, M. Maroliya, and S. K. Saha, “Numerical investigation and optimisation of solid-solid PCM based plate fin heat sinks for electronic cooling,” Appl. Therm. Eng., vol. 248, p. 123183, 2024.

[19] B. Praveen and S. Suresh, “Experimental study on heat transfer performance of neopentyl glycol/CuO composite solid-solid PCM in TES based heat sink,” Eng. Sci. Technol. Int. J., vol. 21, pp. 1086–1094, 2018.

[20] V. C. Midhun and S. K. Saha, “Solid-solid phase change material composite based heat sink with tandem coupled heat pipes for thermal management of electronics,” Appl. Therm. Eng., vol. 267, p. 125846, 2025.

[21] A. Serrano, J.-L. Dauvergne, S. Doppiu, and E. Palomo Del Barrio, “Neopentyl glycol as active supporting media in shape-stabilized PCMs,” Materials, vol. 12, no. 19, p. 3169, 2019.

[22] K. V. Jithin and P. K. Rajesh, "Numerical analysis of single-phase liquid immersion cooling for lithium-ion battery thermal management using different dielectric fluids," Int. J. Heat Mass Transf., vol. 188, p. 122608, 2022.

[23] D. Velliadou, K. D. Antoniadis, A. N. Assimopoulou, M. J. Assael, M. C. M. Sequeira, and W. A. Wakeham, "Accurate measurements of the thermal conductivity of n-docosane, n-tetracosane, 1,6-hexanediol, and 1,8-octanediol in the solid and liquid phases," Int. J. Thermophys., vol. 44, no. 5, 2023.

[24] ANSYS Inc., ANSYS Fluent Theory Guide, 2020. [Online]. Available: https://www.ansys.com

[25] G. H. Kim, K. Smith, K. J. Lee, S. Santhanagopalan, and A. Pesaran, "Multi-domain modeling of lithium-ion batteries encompassing multi-physics in varied length scales," J. Electrochem. Soc., vol. 158, 2011.

[26] N. O. Moraga, J. P. Xaman, and R. H. Araya, "Cooling Li-ion batteries of racing solar car by using multiple phase change materials," Appl. Therm. Eng., vol. 108, pp. 1041–1054, 2016.

[27] V. R. Voller and C. Prakash, "A fixed grid numerical modelling methodology for convection-diffusion mushy region phase-change problems," Int. J. Heat Mass Transf., vol. 30, pp. 1709–1719, 1987.